Data Analysis of the Floating Potential Measurement Unit aboard the International Space Station

Dr. Aroh Barjatya*
Assistant Professor, Physical Sciences
Embry-Riddle Aeronautical University,
Daytona Beach, FL 32114

Dr. Charles M. Swenson
Professor, Electrical and Computer Engineering
Utah State University, Logan, UT 84322

Dr. Donald C. Thompson
Research Associate Professor,
Center for Atmospheric and Space Sciences
Utah State University, Logan, UT 84322

Dr. Kenneth H. Wright, Jr.
Research Scientist, Center for Space Plasma and Aeronomic Research
University of Alabama in Huntsville, Huntsville AL 35899

Abstract

We present data from the Floating Potential Measurement Unit (FPMU), that is deployed on the starboard (S1) truss of the International Space Station. The FPMU is a suite of instruments capable of redundant measurements of various plasma parameters. The instrument suite consists of: a Floating Potential Probe, a Wide-sweeping spherical Langmuir probe, a Narrow-sweeping cylindrical Langmuir Probe, and a Plasma Impedance Probe. This paper gives a brief overview of the instrumentation and the received data quality, and then presents the algorithm used to reduce I-V curves to plasma parameters. Several hours of data is presented from August 5^{th}, 2006 and March 3^{rd}, 2007. The FPMU derived plasma density and temperatures are compared with the International Reference Ionosphere (IRI) and USU-Global Assimilation of Ionospheric Measurement (USU-GAIM) models. Our results show that the derived in-situ density matches the USU-GAIM model better than the IRI, and the derived in-situ temperatures are comparable to the average temperatures given by the IRI.

PACS numbers:

*Electronic address: Aroh.Barjatya@erau.edu

The Floating Potential Measurement Unit (FPMU) was developed by Utah State University's Space Dynamics Laboratory (USU-SDL) to study surface charging of the International Space Station (ISS). The surface charging of the ISS is a complex problem owing to its large size, its variety of conductive/dielectric areas, and the exposed solar cell edges on its high voltage solar arrays. Not only is severe charging of the ISS a hazard for astronauts on Extra Vehicular Activity, but any resultant surface arcing can lead to functional anomalies and surface degradation on the ISS. Thus, the FPMU was developed under intense oversite and reporting requirements as it was deemed critical for ISS safety operations.

Although the primary purpose of the FPMU remains to monitor charging levels of the ISS and provide a dataset that can be used to validate the ISS charging models [1], a secondary purpose is the measurement of electron density and temperature within the F-region of the ionosphere to aid in the understanding of why the ISS charges. Unfortunately, the FPMU is not operated continuously. It is activated by ground commands and data is recorded only for specific data campaign durations. Thus, it is essentially a "snapshot" instrument for ionospheric density and temperature measurements.

Presented in the remainder of this section is a brief overview of the FPMU instrument suite. The next section presents the acquired data quality and the steps taken to compensate for noise and errors. This is followed by descriptions of the data processing algorithms to reduce the acquired data to plasma parameters such as electron and ion density (n_e and n_i) and electron temperature (T_e). We conclude the paper with a discussion and comparison between the FPMU derived plasma parameters and those derived from the International Reference Ionosphere (IRI) model and the Utah State University - Global Assimilation of Ionospheric Measurements (USU-GAIM) model.

As illustrated in figure 1, the FPMU is an instrument suite comprising of four separate instruments [2–4]. Three of the instruments are based on Langmuir probe or DC electrical properties, while a fourth instrument is based on the radio-frequency (RF) properties of the probe.

The Floating Potential Probe (FPP) is a gold-plated sphere of radius 5.08 cm. The sphere is isolated from the chassis ground by a high impedance circuit $\geq 10^{11}$ ohms. The FPP measures the ISS floating potential (ϕ_{fISS}) at the FPMU location within a range of -180 to +180 V at 128 Hz. The Wide-sweeping Langmuir Probe (WLP) is also a gold plated sphere of radius 5.08 cm and is swept with a triangular wave from -20 to +80 V relative to

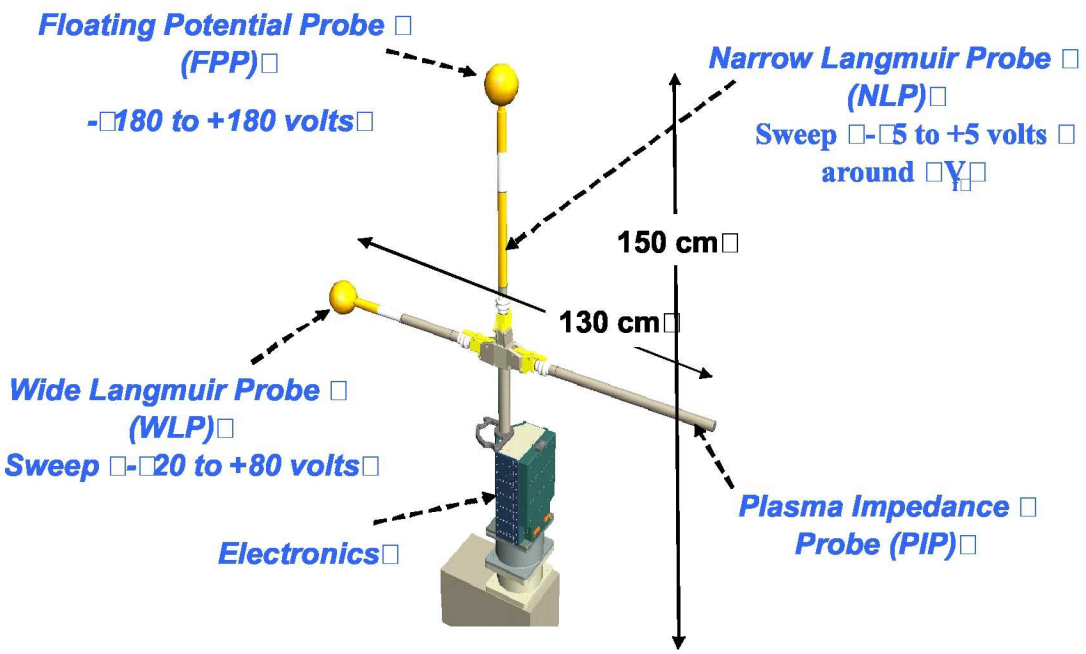

FIG. 1: Floating Potential Measurement Unit (FPMU) conceptual instrument layout.

the chassis ground (i.e. the ISS structure) in 2048 voltage steps. The up-sweep is followed by a down-sweep of equal amplitude and sample length. The current resulting from the applied voltage sweep is measured on two different 12-bit channels: the low-gain channel and the high-gain channel. The WLP low gain channel has a resolution of 700 nA and the high gain channel a resolution of 3.5 nA per count of ADC. Thus, the high-gain channel has sufficient sensitivity to observe both photo emission and ion collection currents, and the low-gain channel is optimized for observing thermal electron currents. The Narrow-sweeping Langmuir Probe (NLP) is a gold-plated cylinder with radius 1.43 cm and length 5.08 cm. The NLP is placed mid-way on the boom supporting the FPP and is guarded on each side by gold-plated cylinders with radius 1.43 cm and length 10.2 cm that are swept in synchrony with the NLP. A sweep from -4.9 to +4.9 V, in 512 equal steps, is applied to the NLP during one second, followed by a sweep down from +4.9 to -4.9 V the next second. This sweep voltage is referenced to the floating potential as measured by the FPP. Thus, even this small sweep range should cover the electron retardation region and some electron saturation region, enabling determination of n_e and T_e at 1 Hz. The resulting current is again measured on two channels with different gains. The NLP low gain channel has a resolution of 175 nA and the high gain channel a resolution of 0.88 nA per count of ADC. The ground based

laboratory calibration of the instrument showed that the WLP and NLP instrument noise was limited to just quantization errors.

The Plasma Impedance Probe (PIP) consists of an electrically short dipole antenna that is electrically isolated from the ISS. It is operated in two different modes. In the Plasma Sweeping Probe (PSP) mode, the instrument measures the electrical impedance (magnitude and phase) of the antenna at 256 frequencies over a 100 KHz to 20 MHz range. In the Plasma Frequency Probe (PFP) mode, the antenna tracks the frequency at which an electrical resonance associated with the upper-hybrid frequency occurs.

To minimize any interference between individual instruments the probe surfaces were set at least two Debye lengths apart for a worst-case rarified and cold ionospheric plasma. The tip-to-tip distance from the WLP to the PIP is 130 cm and the whole instrument stands about 150 cm tall. The FPMU interfaces with the ISS through the Video Distribution System (VDS) similar to an External TV Camera Group on the ISS. Thus, essentially the structural, electrical and communication interfaces of the FPMU with the ISS replicate an external video camera.

The FPMU was carried to the ISS on STS-121 and deployed on August 3, 2006, on the starboard (S1) truss of the ISS. Since its deployment there have been several data acquisition campaigns throughout 2007. Only the dataset from August 2006 and March 2007 campaign is presented in this paper.

I. DATA QUALITY AND PRE-PROCESSING

There are several factors that affect the quality of the FPMU dataset. We shall look at three different noise and error sources: telemetry system errors in data transmission and decoding from the ISS VDS, noise due to interference from other systems on the ISS, and errors due to contamination or non-uniform work function of probe surface.

Data from the FPMU is formatted and distributed as a video signal through the ISS VDS and is recovered at the NASA Johnson Space Center's ISS Mission Control Center. In order to detect any noise induced in the data during transmission, the FPMU telemetry page has inbuilt checksums. Each telemetry page is divided into seven frames with a 32-bit CRC checksum calculated for each frame onboard the ISS and included within the frame. Thus, the first indication of noise in the dataset (noise that is not instrument related) comes

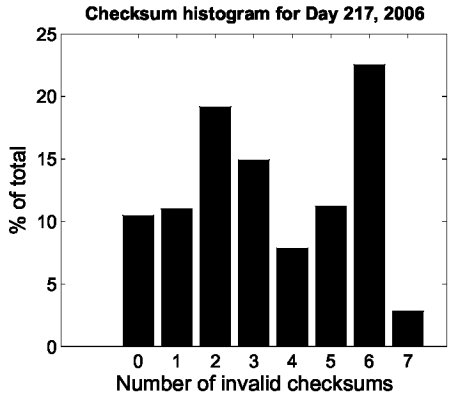

FIG. 2: Histogram of the number of invalid checksums when recalculated over the received page on the ground station. A value of 0 means all seven checksums were valid and the page were received uncorrupted.

when the checksum value included within the frame does not match the checksum value calculated on the ground for the received frame. Figure 2 shows a histogram of the number of invalid checksums per telemetry page for day 217 (August 5^{th}) 2006. Only 10.4% of the received telemetry pages were uncorrupted. An example dataset from all four instruments for a telemetry page with six out of seven checksums being invalid when recalculated on the ground station is shown in figure 3. As can be seen most of the noise in the WLP and the NLP I-V curves seems to be a bit-slip, hence, doubling (sometimes quadrupling), or halving the actual value. The telemetry noise for the FPP one second dataset shows the value to rail to the bottom of its operating range, i.e. -180 V. The telemetry noise in the magnitude channel of the PSP appears to be random.

We mitigate the effect of this noise by running a 7-point median filter through the WLP, NLP, and PSP sweeps. The FPP was sampling the ISS floating potential at 128 Hz. We reduce the sampling to 1 Hz by running a median filter over the entire one second sample set. The resultant filtered data is shown in green in figure 3.

Even for sweeps that were not affected by any VDS induced noise (i.e. all onboard calculated checksums were valid after reception at ground), the electron saturation region for the WLP and the NLP I-V curves is still noisy for intermittent time periods. Figure 4 shows unfiltered I-V curves from two different time periods for telemetry pages with all seven valid checksums. The I-V curves from 12:20:45 UTC are noisier than those from 06:58:26 UTC. We believe this noise to be due to interference from some other apparatus or activity

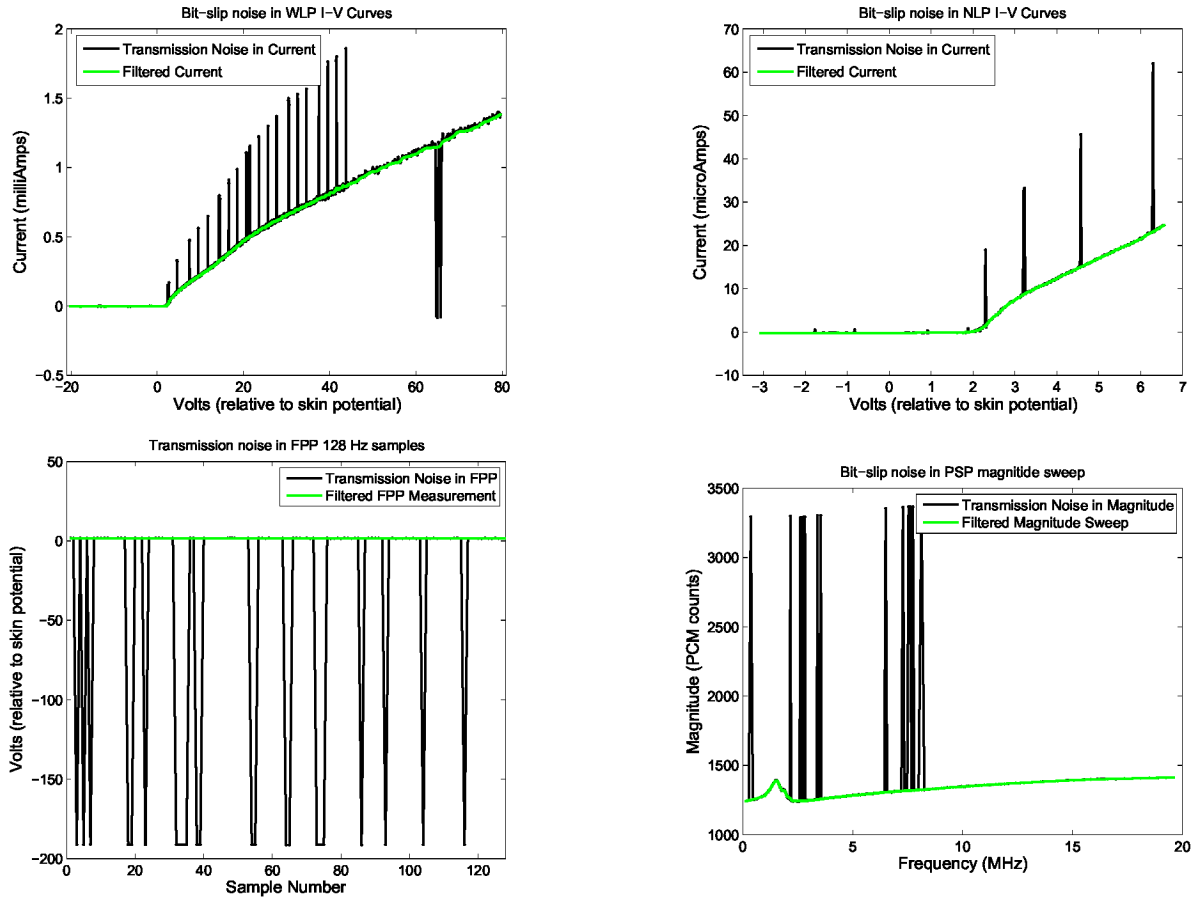

FIG. 3: Noise in the dataset of all four FPMU instruments due to telemetry errors. Median filtering mitigates most of the "spikes."

onboard the ISS that occurs intermittently, thus, also affecting the FPMU intermittently. Any effect of this noise seems to be significant only for the electron saturation region and we expect to be able to derive plasma density and temperature from the ion saturation and electron retardation region without any significant problems.

It is interesting to note that the cylindrical NLP shows a "negative" characteristic in electron saturation region at the very top of the sweep for the curve from 12:20:45 UTC. This feature is observed in both the up-sweep as well as the down-sweep over long periods of time. Dote and Amemiya [5] have reported on such "negative" characteristic observations for cylindrical probes in strongly magnetized (hundreds of Gauss) plasma chambers. Rubinstein and Laframboise [6] have also theoretically predicted this feature for magnetized plasmas dependent on the strength and alignment of the magnetic field. However, in both of those cases, the "negative" characteristic occurs at plasma potential (ϕ_p), while we observe it

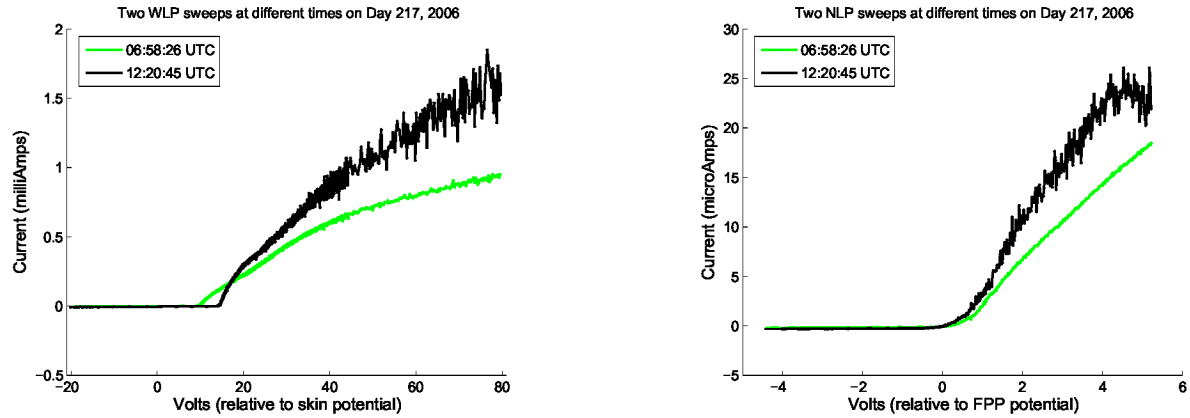

FIG. 4: Noise in the WLP and the NLP I-V curves possibly due to interference from some other apparatus or activity onboard the ISS. Both curves are from when ISS was in eclipse conditions. The difference in floating potential observed in WLP curves is because of ISS charging due to VxB effect.

well into the electron saturation region. This phenomenon in electron saturation region has also been seen on two separate rocket flights carrying heated cylindrical sweeping Langmuir probes [7]. At this time no satisfactory explanation for this phenomenon exists.

The effects of contamination and non-uniform work function of the probe surface on the measured I-V curves have been previously studied [8, 9]. The predominant effect has been described as the presence of hysteresis in the I-V curves as the voltage is swept up and down in a triangular waveform. This hysteresis is indicative of a disturbed retardation region leading to anomalously high electron temperature retrievals. Both the WLP and the NLP were gold plated to provide a uniform work function for the probe surface as well as to provide some stability in the corrosive atomic oxygen environment of Low Earth Orbit. Additionally the WLP can be heated with a small halogen lamp that was placed inside the hollow sensor sphere. The lamp is powered on and off from ground commands. The temperature of the WLP surface is a function of solar beta angle to the ISS. Without internal heating the temperature of the WLP surface will range from -58°C for low beta to 118°C for high beta. When the internal heater is turned on the temperature of the probe will approach 350°C after several orbits. This heating was done to boil off any contaminants from the probe surface [10, 11]. Figure 5 shows four consecutive filtered sweeps from the WLP which clearly show the absence of hysteresis, and hence a clean probe surface. The NLP was not internally heated and is expected to clean its surface with heat from the Sun.

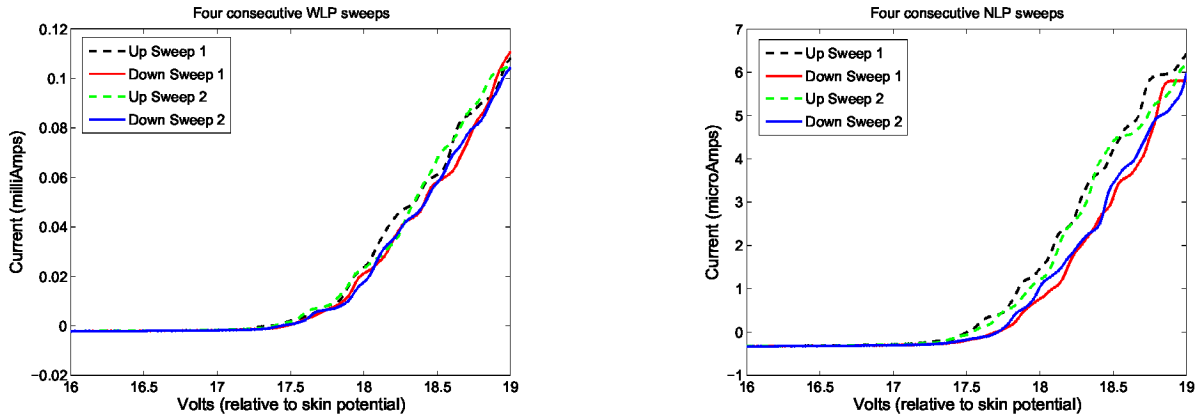

FIG. 5: Four consecutive I-V curves from the WLP and the NLP. There is no hysteresis in the internally heated WLP, while minimal hysteresis exists in the NLP indicating presence of some contamination.

Figure 5 also shows four consecutive filtered sweeps of NLP at the same instant as that of the WLP. Only a minimal presence of hysteresis is visible in the NLP I-V curves.

II. DATA PROCESSING: DERIVING n_i, n_e, AND T_e FROM THE WLP AND THE NLP DATASET

Langmuir probes were first used as diagnostic tools for plasma chambers by Irving Langmuir in the early 20^{th} century [12, 13]. Since then, the Langmuir class of electric probes has also been used on many sounding rockets, satellites, and inter-planetary spacecrafts to perform in situ measurements of plasma parameters such as electron density (n_e) and temperature (T_e), ion density (n_i), and as an indicator for spacecraft charging. We present a brief overview of the various analytic expressions that have been presented in the literature to describe the collected current by a Langmuir probe under various conditions. Unfortunately there are known limitations in the use of these expressions for flowing, magnetized and collisional plasmas, all of which are typically encountered when analyzing Langmuir probe data obtained from suborbital rockets and satellites. Detailed Langmuir probe theory can be read from several references [14–17].

A. Review of Langmuir Probe Current Collection Expressions

The random thermal current to a surface for a charge species q_j primarily depends on the density (n_j), temperature (T_j), and mass (m_j) of the charge species, and the surface area (A) of the probe:

$$I_{th_j} = n_j q_j A \sqrt{\frac{k_B T_j}{2\pi m_j}}, \tag{1}$$

where k_B is the Boltzmann constant. While equation 1 governs the random current collected by a conducting surface at the potential of the surrounding plasma, a typical Langmuir probe collects current over a range of applied potentials. The resulting I-V curve can be divided into three regions of operation: electron retardation, ion saturation, and electron saturation. These regions are roughly divided by the plasma potential and the floating potential, and are named after the dominant collected charged species over that range of applied potentials. The plasma potential, ϕ_p, is the potential at which no electric fields exist between the probe and the plasma and the only current collected is the thermal current of the charge species, while the floating potential, ϕ_f, is the potential attained by a probe such that the total current of various charge species to the conducting surface sums to zero. The first region to be discussed is the electron retardation region that refers to the part of I-V curve that lies between ϕ_f and ϕ_p. In this region thermal electrons are repelled and ions are attracted. Despite being repelled, electrons are still the dominant collected species and the ions constitute only a minor portion of the collected current. For plasma with Maxwellian velocity distribution, the electron current in this region is exponential with probe potential and is scaled by the electron thermal current. It is given by

$$I_e(\phi) = I_{th_e} \exp\left(\frac{e(\phi - \phi_p)}{k_B T_e}\right), \tag{2}$$

where ϕ is the potential applied to the probe relative to ϕ_p, e is the fundamental electron charge and I_{th_e} is the electron thermal current given by equation 1. Note that the current "from" the probe (i.e. electron collection) is referenced as positive in the presented equations.

The current collected in either the electron or ion saturation regions for a non-drifting, unmagnetized, and collisionless plasma, when the probe dimensions are much smaller than the Debye length, is given by the Mott Smith-Langmuir Orbital Motion Limited (OML)

theory [13] and is represented by

$$I_j(\phi) = I_{th_j}\left(1 + \frac{q_j(\phi - \phi_p)}{k_B T_j}\right)^{\beta}, \tag{3}$$

where

$\beta = 0$ Planar probe,

$\beta = 1/2$ Cylindrical probe,

$\beta = 1$ Spherical probe.

The parenthesized expression in equation 3 signifies the increase in collection current with the growth in effective collection area as the potential structure around curved probes changes when $|\phi - \phi_p| > 0$. It is important to differentiate this effective collection area from the term A in equation 1 which represents the physical surface area of the probe in contact with the plasma.

The saturation region theory becomes complicated as each of the above assumptions (non-drifting, unmagnetized, and collisionless) about the state of plasma are violated. In the case of spacecraft motion through plasma (i.e. plasma drift relative to probe) the thermal speed of ions is usually less than the spacecraft speed while the electron thermal speed is higher than the spacecraft speed. This situation is generally referred to as "mesothermal" plasma and primarily affects the ion saturation region. An approximate equation for the ion saturation current for a cylindrical Langmuir probe [18] is given by

$$I_i(\phi) = I_{th_i}\frac{2}{\sqrt{\pi}}\left(\frac{m_i v^2}{2k_B T_i} + \frac{1}{2} + \frac{q_i(\phi - \phi_p)}{k_B T_i}\right)^{\frac{1}{2}}, \tag{4}$$

where v is the spacecraft velocity, and ϕ is the applied probe potential. The first term is the ion "ram" current and is the dominant term at orbital velocities. The other two terms refer to thermal motion and increase in collection due to attractive potentials, respectively. At orbital velocities the mesothermal situation creates a rarefied wake region behind the probe, thus, the surface area A in contact with plasma is the probe area projected normal to v.

Although one would expect that the electrons (having a much higher speed than the spacecraft) can still approach the probe from all directions, this is generally not so. The electrons can only penetrate into the ion wake region as much as ambipolar diffusion would allow, thus the mesothermal condition is expected to affect even the electron collection

current. Katz et al. [19] have reported that for a mesothermal plasma a spherical probe collecting in the electron saturation region fits equation 3 with $\beta = 0.5$, which is unlike the value of β that OML theory predicts. Similarly, Piel et al. [9] also reported that their spherical probe observations aboard a sounding rocket fit equation 3 the best with $\beta = 0.58$.

With the addition of magnetic field the charged particle motion around the probe is constrained by the particle's gyro-radius and the alignment of the probe with respect to the magnetic field. The situation is best described as a "magnetic bottle" (see figure 6 of Rubinstein and Laframboise [6]). Parker and Murphy [20] first tackled the problem of current collection in magnetized plasma by neglecting particle thermal motion in addition to the assumption of nondrifting collisionless plasma. This effectively gives a canonical upper bound to the collected saturation current and is given by

$$I_j(\phi) = \frac{I_{th_j}}{2}\left(1 + \left(\frac{8\,|q_j(\phi - \phi_p)|}{m_j\omega_j^2 r^2}\right)^{\frac{1}{2}}\right), \tag{5}$$

where ω_j is the particle gyrofrequency and r is the probe radius. The calculation of the upper bound that includes the particle thermal motion is further complicated and was done by Rubinstein and Laframboise [6]. A simplified version in the limit of large attractive potentials is given by

$$I_j(\phi) = I_{th_j}\left(\frac{1}{2} + \frac{1}{2}\left(\frac{8\,|q_j(\phi - \phi_p)|}{m_j\omega_j^2 r^2}\right)^{\frac{1}{2}} + \frac{k_B T_j}{m_j\omega_j^2 r^2}\right). \tag{6}$$

The first two terms are the same as Parker and Murphy equation. The last term is a result of orbital motion of the particles and vanishes for strong magnetic fields.

An asymptotic analysis of the effect of collisions in a non-drifting magnetized plasma has been done by Sanmartin [21]. However, due to the complexity involved, collisions in a magnetized plasma are generally ignored. Early computer simulation programs (NASCAP /LEO and POLAR) have shown the collisionless approximation to be good to within 5% [22] under low Earth orbit ionospheric conditions. The most complicated situation arises in the case of mesothermal magnetized plasma. Thompson's work on electrodynamics of conducting tethers in LEO [23] has treated this problem with a collisionless assumption, and shows that drifting effects cannot be ignored for electrons even if their thermal motion is much faster than the drift speed. There is however presently no theory for quantitative

calculations of collected current in mesothermal magnetized plasma [24], short of a computer particle-in-cell (PIC) simulation.

B. Algorithm to Reduce the WLP and the NLP I-V Curves to Plasma Parameters

As discussed in the previous subsection, Langmuir probe theory is complex in the case of mesothermal magnetized plasma, a situation seen by probes on spacecrafts in low Earth orbit in the ionosphere. However, knowledge of the spacecraft orbital parameters and expected ionospheric plasma parameters can improve approximations during data analysis, thus making the problem tractable.

The ISS orbital speed is on an average about 7.4 km/s, its altitude is approximately 350 km, and the orbit inclination of 51.63 degrees is such that it rarely crosses into high latitude auroral conditions. The average thermal speed for O^+ ions at 2000 °K, a maximum expected ion temperature at the ISS orbit altitude, is about 1.8 km/sec, which is significantly below the ISS orbital velocity. Thus, the predominant component of ion current at ϕ_p is expected to be the ram current. With the knowledge of the ISS velocity, probe cross section area, and the location of ϕ_p within the I-V curve, one can thus determine the ion density. The accuracy of the calculated n_i is limited only by the accuracy with which we determine ϕ_p. Furthermore, the accurate determination of temperature from the retardation region and determination of density from the saturation region are also significantly dependent on knowing the potential applied to the probe relative to the ϕ_p.

Thus, the single most important step in analyzing any Langmuir probe I-V curve is to first find the plasma potential, ϕ_p. In an ideal situation, ϕ_p is the point where the curve characteristics deviate from an exponential form, a point generally referred to as the "knee" in the I-V curve. However, both Sanmartin [21] and Rubinstein and Laframboise [6] have shown that in a magnetized plasma there is a decrease in collected current near the plasma potential thereby producing a "rounding of the knee" effect in the region where the I-V curve transitions from electron retardation to electron saturation region. Thus, determining ϕ_p as the last point that fits an exponential curve would be erroneous. Consequently we use an iterative procedure to determine ϕ_p.

In the first step we fit a line in the ion saturation region and subtract that from the total collected current. This approximately gives the electron collection current. We then

take the first derivative of the electron current with respect to voltage. The location of the maxima within $dI_e/d\phi$ gives a very crude approximation of ϕ_p, akin to finding the "knee." We do not expect the plasma temperature to be larger than 5000°K, and thus we limit the search for the maxima to within 1.0 eV of ϕ_f, enough for the retardation region to transition into saturation region. The value of ϕ_f is determined by the point where the total collected current goes to zero. This limited point search avoids erroneous recognition of noise spikes that occur far from ϕ_f as the "knee." At plasma potential the OML ion saturation current is a much smaller component than the ion ram current to the total ion collection current, therefore, by equating the value of the ion collection current linear fit at the location of ϕ_p to the ion ram current we get a first order approximation to the ion density.

In the second step, we assume the plasma to be quasineutral and do a nonlinear least squares curve fit of the total collected current to

$$I_{total}(\phi) = -n_i e A V_{ISS} + I_{th_e} \exp\left(\frac{e(\phi - \phi_p)}{k_B T_e}\right), \tag{7}$$

which is just a combination of the ion ram current and electron retardation current, and where $n_i = n_e$, A is the probe ram projected area, and V_{ISS} is the ISS orbital velocity. This equation follows an idea similar to that behind equation 4. We use the density as calculated in the first step and fit equation 7 in a least square sense for only T_e and ϕ_p. This nonlinear fit is done only for points within ϕ_f-0.35 eV to ϕ_f+0.08 eV. The fit is done for the limited range of points because the farther positive relative to ϕ_f we go, the more the electron current is expected to deviate from an exponential form, and the farther negative we go the more the ion OML current becomes dominant. This nonlinear fit gives a much more accurate value of ϕ_p. Figure 6 shows the fits for typical WLP and NLP sweeps. We neglect photoelectron effects as it should only constitute a small current to the ion saturation region due to the expected high thermal plasma density at the ISS orbital altitudes.

We then further refine the value of n_i by evaluating the ion saturation current line fit at the ϕ_p determined in second step. Having now ascertained a much more accurate value of ϕ_p, we also make a second attempt at calculating the value of T_e by using the traditional method of line fits to the logarithm of the electron current for voltages below ϕ_p. This method generally corroborates the T_e values determined in the second step, however, the standard deviation of T_e values determined by this method is found to be slightly larger than that of values determined in the second step.

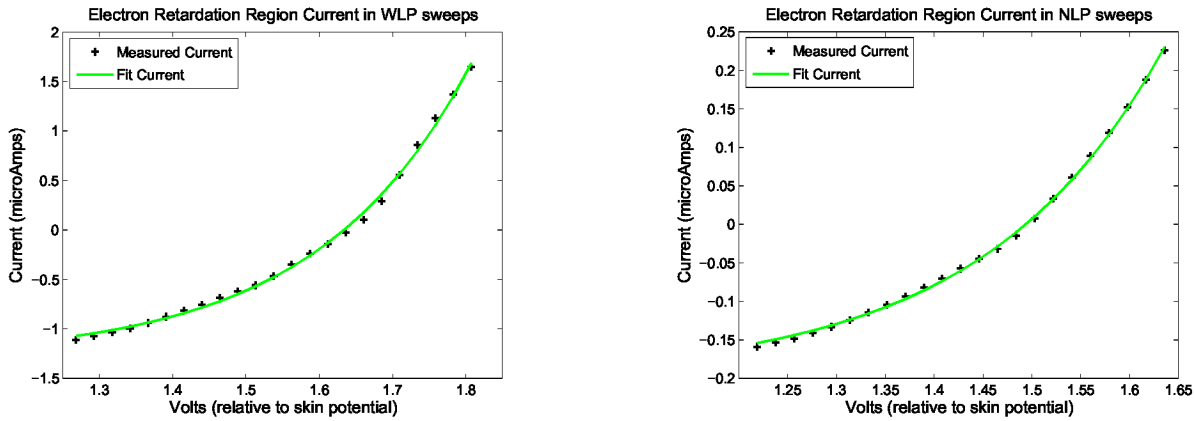

FIG. 6: Fits for T_e and ϕ_p to the electron retardation region using equation 7. Both the WLP and the NLP I-V curves are for the same second of data. The T_e and ϕ_p fits for the WLP I-V curve were 2420 °K and 2.12 V, while for the NLP I-V curve were 2670 °K and 2.01 V, respectively.

With the accurate knowledge of the plasma potential we can also compare the observed electron saturation region to the various current collection theories. Figure 7 compares the actual WLP and NLP I-V curves with the curves made from various current collection theories using the plasma density and temperature as derived in the previous steps. As is seen, none of the equations presented in the previous subsection even come close to the observed current. We then fit equation 3 to the observed current in a least squares sense for n_e and β using the values of T_e and ϕ_p as derived in second step. The nonconformity of the fitted β values to those that the OML theory proposes is expected as the FPMU Langmuir probes are comparable and even larger than the Debye length at the ISS orbital altitudes. Furthermore, it is important to note that as per equation 3, the collected electron current is directly proportional to the density as well as the probe surface area A in contact with plasma. The accuracy of the fit for density, thus, depends on the accuracy of assumed surface area of the probe that is in contact with plasma. Initially the term "A" in the equation was taken to be the entire surface area of the probe. Although the subsequently acquired fit matched the observed current very well in the electron saturation region, the fit value of n_e is lower than the value of n_i that was calculated earlier. We believe this to be due to wake effects, wherein the portion of the probe surface that actually collects electrons is less than the entire surface area of the probe. Consequently, if we take the current collection surface area for the electron saturation current to be equal to only the surface area that is projected in the ram direction, then the value of n_e comes to within $\pm 10\%$ of the n_i value.

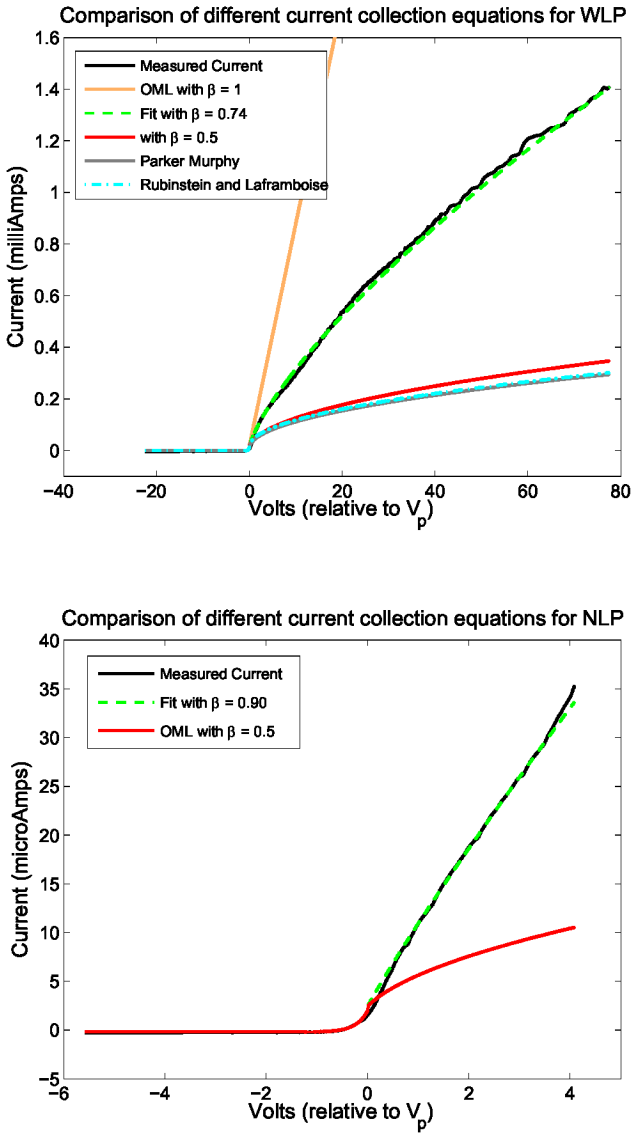

FIG. 7: Comparison of measured I-V curves with the I-V curves generated by analytical theory. The best match is acquired with a least squares fit of equation 3 to n_e and β. It is important to note that the fit value of β is different from that proposed by OML theory.

Thus, in the third step of WLP and NLP I-V curve data analysis, we derive electron density from the electron saturation region by fitting equation 3 for n_e and β assuming that only the projected probe surface area is in contact with plasma. The actual surface area that is in contact with plasma is expected to be larger than just the projected surface area due to minor ambipolar diffusion within the wake to the probe's anti-ram side. This additional area is assumed to be small but is expected to vary throughout an orbit. The value of n_e thus derived is not expected to be very accurate, unless a PIC simulation of wake effects is

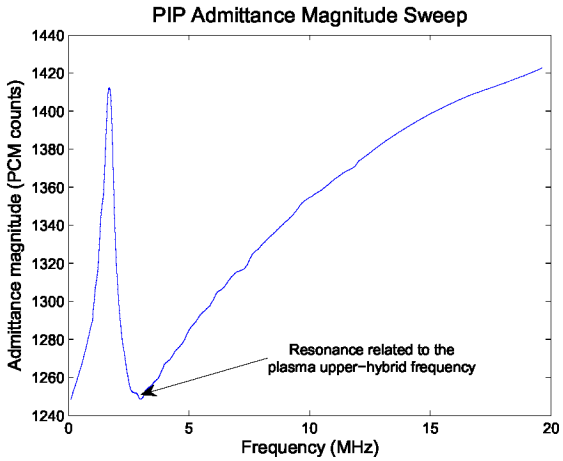

FIG. 8: A single admittance vs. frequency profile from the PIP dataset.

done to accurately determine the area in contact with plasma.

III. DATA PROCESSING: DERIVING n_e FROM THE PIP DATASET

The impedance characteristics of an antenna immersed in an ionospheric plasma were first used by Jackson [25] to determine ionospheric electron density in the late 1950's. Since then, there have been several significant efforts in further development of the theory [26–28] and in advancing the experimental technique [29–32].

The principle behind the operation of an impedance probe is simple: the input impedance of an electrically short antenna immersed in a plasma varies and can be observed as the antenna is swept with a changing radio-frequency (RF) source. The observed impedance vs. frequency profile shows strong features as the antenna resonates with the fundamental plasma frequencies. The impedance profile achieves a minima near the electron cyclotron frequency, behaving like a series RLC tuned circuit, and achieves a maxima near the plasma upper hybrid frequency, behaving like a parallel RLC tuned circuit. The impedance vs. frequency profile along with an appropriate theory can then be used to determine various plasma parameters such as electron density, electron-neutral collision frequency, cyclotron frequency, etc. [32]. The most important benefit of an impedance probe is that the antenna input impedance is primarily sensitive only to the dielectric properties of the antenna and is largely independent of the grounding scheme as well as the surface properties of the antenna itself. The technique is thus immune to spacecraft charging.

The PSP operation mode of the PIP measures antenna admittance. An accurate calibration is required to convert the measured admittance (in PCM counts) to impedance in ohms. However, the calibration efforts for the PIP are still incomplete and maybe impossible. A crude measurement of plasma density can still be made based on the location of the parallel resonance (related to upper hybrid frequency) within the admittance profile. A single frequency sweep from the PSP operation mode of the PIP is shown in figure 8. As the PCM counts are a measure of the antenna admittance, the resonance related to the upper hybrid frequency shows up as a trough in the admittance vs. frequency profile. The assumption of upper hybrid frequency as the frequency at which the admittance trough occurs, along with an estimate of cyclotron frequency from the IGRF (International Geomagnetic Reference Field) model, is then used to determine a first-order approximation to electron density. The PFP mode of the PIP is also capable of giving high resolution electron density measurement once the phase locked loop gets locked on the upper hybrid resonance. However, the frequency locks on the upper hybrid resonance have been very sparse, and thus, no data from the PFP will be presented in this paper.

IV. FPMU DATA ANALYSIS RESULTS AND DISCUSSION

Figure 9 presents plasma densities derived from the WLP, the NLP, and the PIP over a several hour long segment on day 217 (August 5^{th}) of 2006. The data dropouts are a result of intermittent Ku-band downlink from the ISS. On August 5^{th} 2006, the acquisition of signal (AOS) was only 38%. The segment of time presented has one of the highest AOS to data drop-out ratio. The results from the analysis of the rest of the dataset are similar in nature. As the figures show, the Langmuir probe derived n_i and n_e values generally agree to within 10%, however, the n_i values have a slightly smaller standard deviation ($\leq$5%) compared to the derived n_e values. This spread in n_e values is largely attributed to the changing collection area of the probes in electron saturation region as well as unavailability of an accurate current collection theory. One measure of confidence we get in our method of least squares fitting for n_e and β over the electron saturation region is that both the WLP and the NLP give the same densities. This is despite the fact that the two probes are of different geometries and that their fits of β vary significantly over the range of 0.5 and 1. The seemingly random variation in the fit values of β indicates that the expression

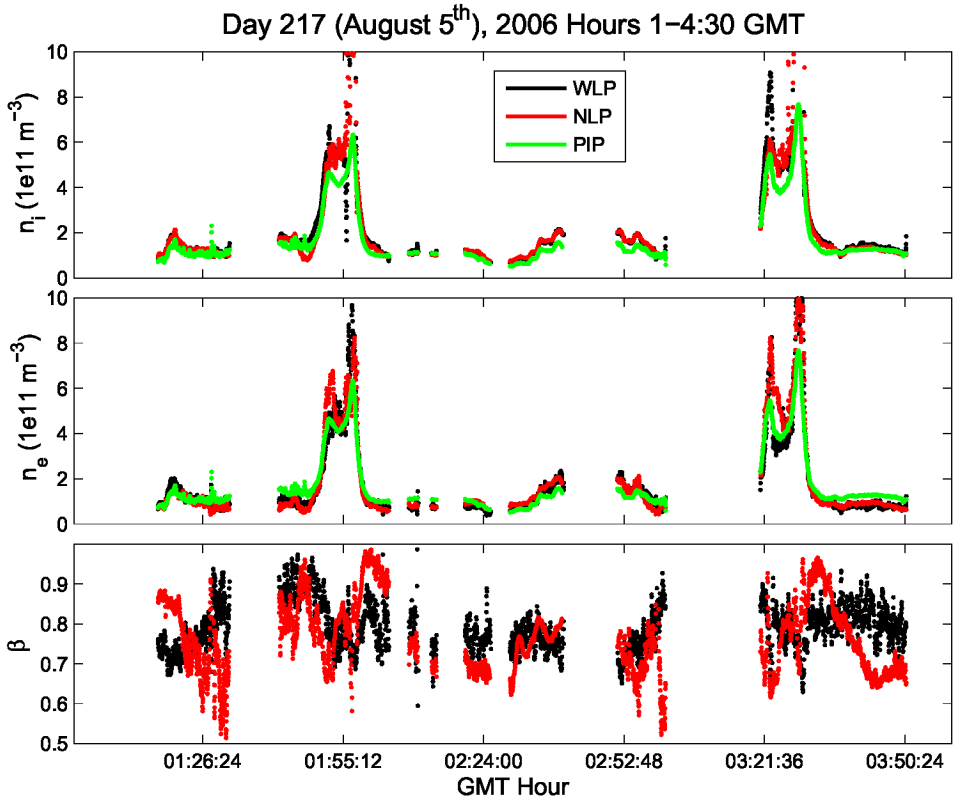

FIG. 9: Comparison of densities derived from different instruments.

$\left(1+\frac{e(\phi-\phi_p)}{k_B T_e}\right)$ is a poor representation of the growth in probe collection area with applied voltage. This can largely be attributed to the fact that the expression is for an isotropic potential distribution around the probe, while in reality, due to the plasma wake in the anti-ram side of the probe, the potential distribution is anisotropic. The large FPMU I-V curve database for two different probe geometries might be of help in determining a more accurate expression.

Although the method used to derive n_e from the PIP dataset is rather crude, the PIP derived n_e generally agrees well with the Langmuir probe derived densities. While the PIP results can be used to confirm the density structure, the derived density itself is found to be always lower than that calculated by Langmuir probes. With the appropriate calibration of the PIP and the subsequent use of an impedance probe theory to derive the density, the PIP results are expected to improve.

The charging of the ISS is a function of ambient plasma density and temperature, the active state of PV solar array, as well as $V_{ISS} \times B$ induced potentials. A model of ISS surface

charging, the Plasma Interaction Model (PIM), has traditionally used plasma densities and temperatures derived from the IRI model to predict the ISS charging levels [1]. The IRI empirical model [33] is an international project that provides users with global and temporal variations of electron density, electron temperature, ion temperature, ion composition (O^+, H^+, He^+, NO^+, O_2^+), ion drift, and Total Electron Content. However, the model only provides average climatologies of the ionosphere parameterized by solar activity, season and geomagnetic activity indices. Due to the nature of parameters the model is based upon, the actual day-to-day variability of the ionosphere can approach up to 30% of the model provided averages [34]. Thus, in situ instrumentation becomes important for high spatial and temporal resolution observations of local plasma parameters that will eventually be used to validate the ISS surface charging model PIM.

The USU-GAIM program is a newer physics-based model of the ionosphere that incorporates a Gauss-Markov Kalman Filter while assimilating a diverse set of near real-time ground based measurements [35]. Due to the data assimilative nature of the model it is expected to be more accurate in ionospheric specification than IRI. However, unlike the IRI model, the USU-GAIM model only provides global electron density and does not produce temperatures. As the USU-GAIM model is fairly new, the FPMU dataset provides an excellent triple redundant measurement of density for comparison and model's validation. Figure 10 shows sites that provided the ground based ionospheric density measurements for assimilation into the GAIM model, the results of which are presented in this paper.

Figures 11 and 12 present data from the FPMU over two several hour long segments on day 217 (August 5^{th}) of 2006 and day 62 (March 3^{rd}) of 2007, respectively. The top rows in both figures show the ISS floating potential at the FPMU location on the ISS structure. Note that the ISS floating potential is plotted as "-$\phi_{f_{FPP}}$", which is a positive number. The figures also compare the plasma density and temperature derived from the FPMU with that generated using IRI and USU-GAIM models. Finally, the ISS latitude and longitude are also presented.

All three instruments (FPP, WLP, and NLP) give the same floating potential to within ± 2 volts, thus meeting the NASA requirements for FPMU success. There are a few outlier floating potential points derived from the WLP and the NLP and are assumed tobe due to noisy I-V curves. Between the two figures, there are three important characteristics discernible in the ISS surface charging: (1) $V_{ISS} \times B$ background due to the motion of ISS

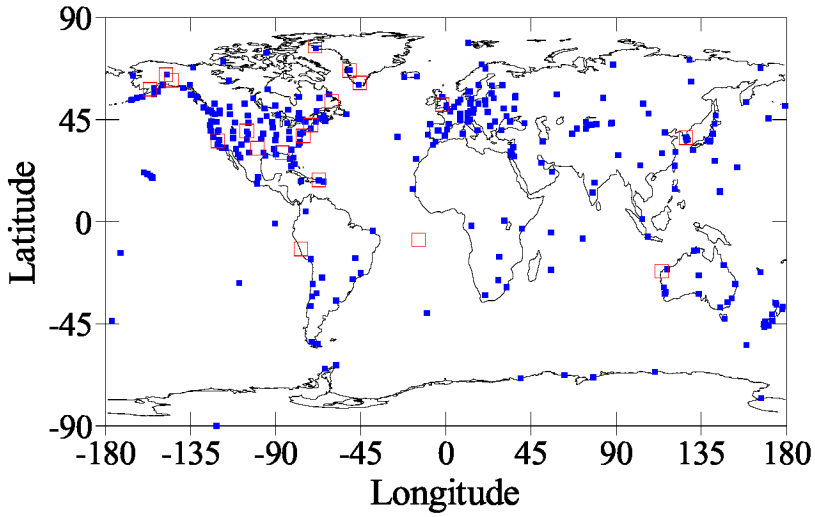

FIG. 10: Ground locations from where the data was assimilated into the USU-GAIM model run. The filled squares are GPS ground stations and empty squares are ionosondes.

through the Earth's geomagnetic field, (2) charging due to additional electron collection on the exposed interconnects of solar cell panels as the ISS passes from eclipse to sunlight, (3) charging due to high densities and low temperatures of the Equatorial Anomaly as the ISS passes through Earth's geomagntic equator region.

The FPMU is located on the extreme end of starboard S1 truss. This location experiences varying degrees of charging due to $V_{ISS} \times B$ as the ISS attitude relative to the Earth's geomagnetic field changes over one orbit. As such, the maximum charging levels of the ISS surface are determined by the location of ISS eclipse exit within the charging profile of $V_{ISS} \times B$. In figure 11 the ISS eclipse exit occurs when the charging due to $V_{ISS} \times B$ is high, thus, taking the overall charging to about -25 V. While in figure 12, the eclipse exit occurs when the $V_{ISS} \times B$ charging at the FPMU location is only a few volts, thus, the overall charging level at eclipse exit in this case is only about -15 V, which is almost entirely due to additional electron current collection on the ISS solar panels. A future paper will delve more into the charging physics of the ISS surface along with PIM simulation results.

As expected, n_i values derived from the WLP agree more with USU-GAIM than with IRI. It is important to note that the USU-GAIM model employs a coarse grid, so the model peak tends to smooth, or average, the sharp anomaly peaks. This is most clearly seen in figure 12 where the model shows a tendency to fill in between the anomalies. The discontinuities in the GAIM density profile are a result of the way data is extracted from the coarse-grid

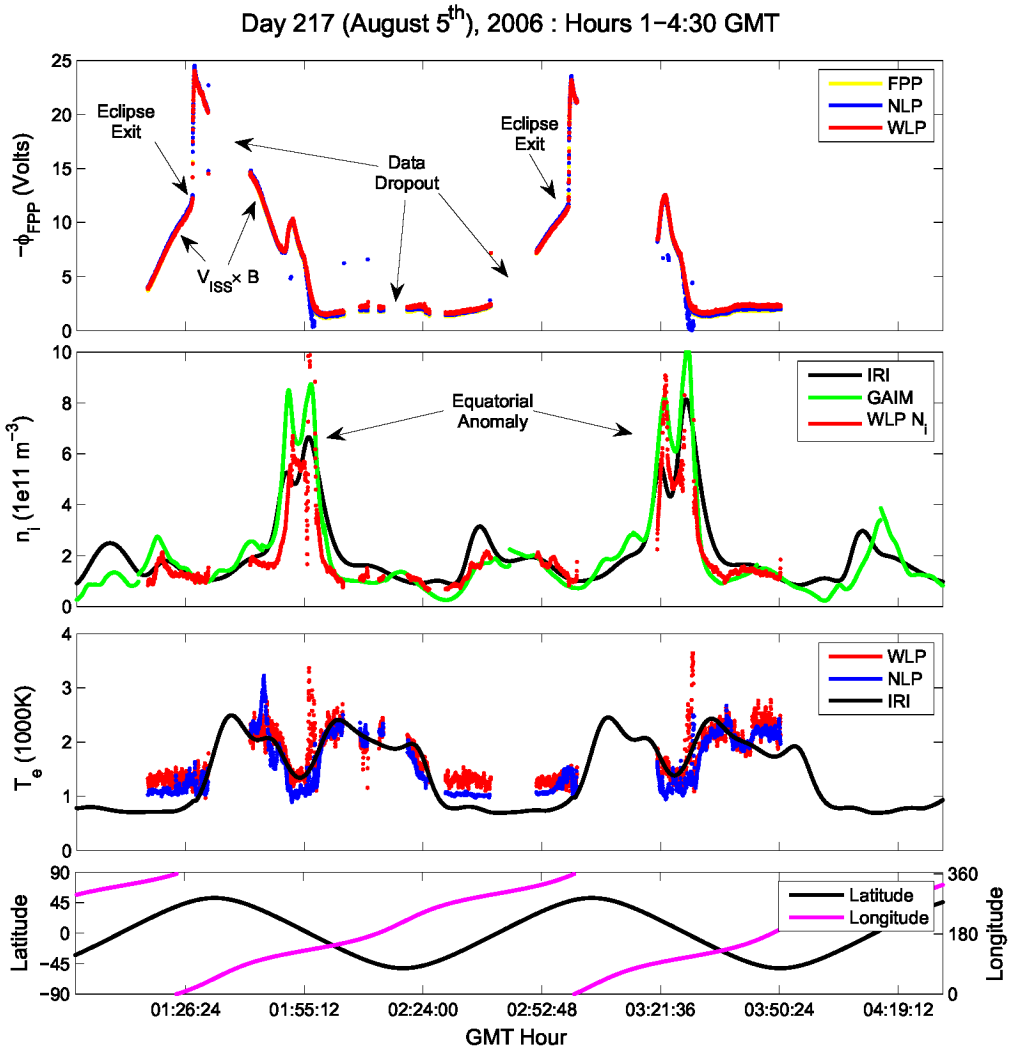

FIG. 11: The first row shows FPMU floating potential as measured by the FPP, the WLP, and the NLP. The second row compares the ion density (n_e) derived from the WLP with density from USU-GAIM and IRI model runs. The third row compares the WLP and the NLP derived temperatures with IRI model results. The fourth row shows the ISS latitude and longitude.

global model. The model produces an electron density specification every 15 minutes. To plot the GAIM density profiles at the exact location of ISS, the density interpolation is done in position but not in time. Thus the extracted data uses the "closest" specification in time. A smooth transition could be obtained by interpolating between two time specifications, as well as in position space, but this hasn't been implemented yet.

Accurate measurement of T_e using Langmuir probes is always difficult. Ferguson et

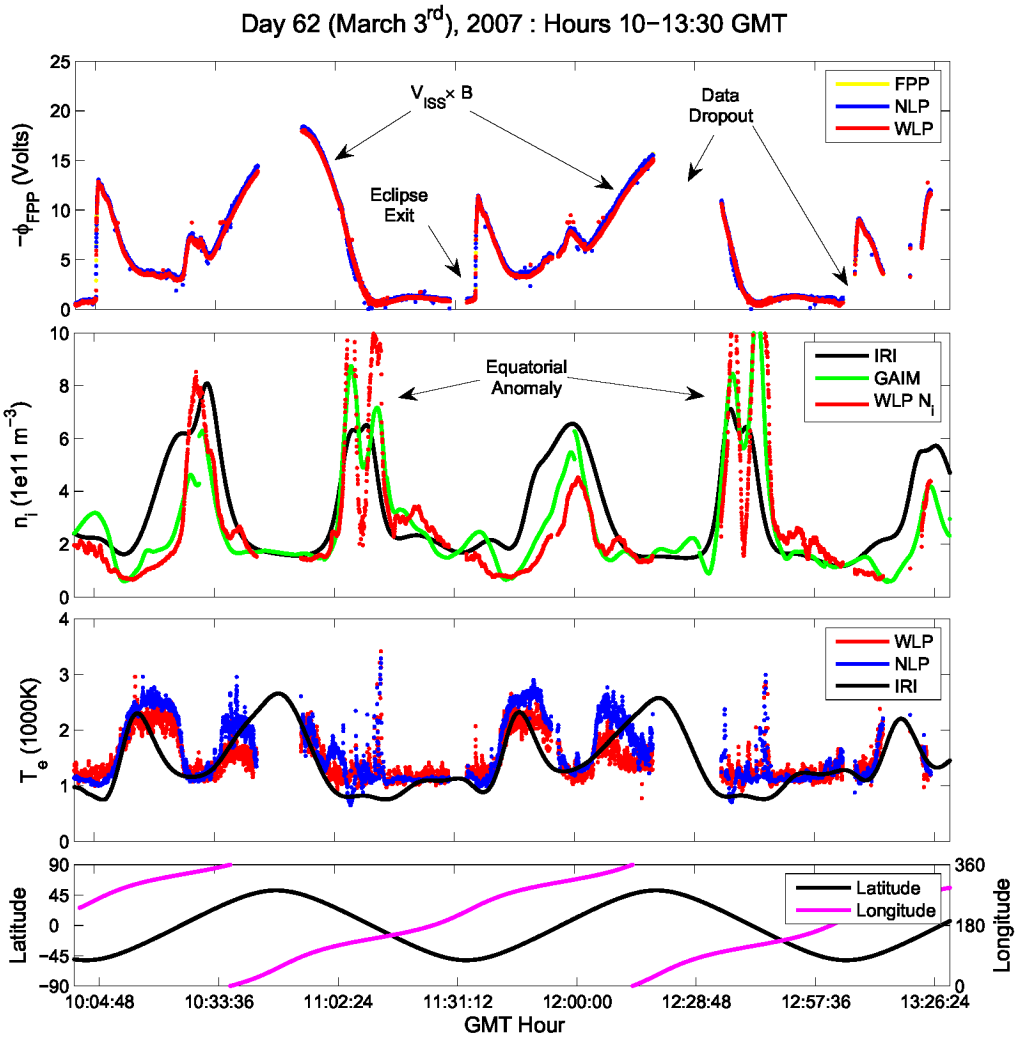

FIG. 12: The caption is the same as for figure 11.

al. [36] analyzed a predecessor instrument suite on the ISS for electron temperatures and reported that the probe reduced temperatures were generally higher than that predicted by the IRI model. In the case of FPMU dataset, although the WLP and NLP derived temperatures have a little spread in values, the general trend does agrees well with the IRI model. At the same time the reduced data also provides small scale features that deviate from the IRI results which should be expected given the averaging nature of the IRI model [34]. For example see the feature around 0330 hrs of day 217, 2006.

V. SUMMARY

The primary objective of the FPMU instrument suite was to provide a triple redundant, "no false alarm", measurement of the ISS floating potential. All three Langmuir probe instruments (FPP, WLP, and NLP) provide the ISS floating potential value to within ± 2 volts of each other, thus fulfilling NASA's requirement of FPMU. The n_i and T_e values provided by the WLP and the NLP also agree to within $\pm 10\%$ of both probes. This provides a doubly redundant measurement that can be used as an input for the ISS charging model or for validation of USU-GAIM model. The first results presented in this paper show that the in situ density measurements agree better with USU-GAIM than with IRI. The derived in situ temperatures are in good agreement with IRI predictions and also show small scale structures that are not visible within the IRI results due to the model's averaging nature.

The FPMU I-V curves from the WLP and the NLP also present an unprecedented dataset where two Langmuir probes of different geometries are probing ionospheric plasma in the same volume. As presented in this paper there is a lack of theory that can be used to accurately analyze the saturation regions of Langmuir probes that do not fall strictly in the OML operation regime and are being operated in mesothermal magnetized plasma. Our analysis of the electron saturation region provides a simple procedure to derive absolute electron density. The accuracy of the derived density values is evident as they agree very well between the two different instrument geometries, as well as with the results from ionospheric models.

The seemingly random variation in the fit value of β points towards the lack of an accurate saturation region current expression. Furthermore, the NLP I-V curves intermittently show a "negative" characteristic in the far electron saturation region that remains unexplained. These topics will be investigated in a future paper. Thus, in the long run, the large FPMU I-V curve dataset shall shed a unique insight into probe physics.

Acknowledgments

The authors would like to thank Dr. Steve Koontz/NASA/JSC for consultation concerning the FPMU flight operations. KHW acknowledges support from NASA through contract

NNM05AA22A.

---

[1] R. Mikatarian, H. Barsamian, J. Kern, S. Koontz, and J. F. Roussel, in *53rd International Astronautical Congress The World Space Congress, Houston, Texas* (2002), pp. IAC–02–T.2.05.

[2] C. M. Swenson, D. C. Thompson, and C. Fish, in *41st Aerospace Sciences Meeting and Exhibit, Reno, Nevada* (2003), pp. AIAA–2003–1081.

[3] C. M. Swenson, D. C. Thompson, and C. Fish, in *8th Spacecraft Charging Technology Conference at Huntsville, Alabama* (2003).

[4] K. H. Wright, C. M. Swenson, D. C. Thompson, A. Barjatya, S. L. Koontz, T. A. Schneider, J. Vaughn, J. A. Minow, P. D. Craven, V. N. Coffey, L. N. Parker, and T. H. Bui, IEEE. Trans. Plasma Sci. **36**, 2280 (2008).

[5] T. Dote and H. Amemiya, J. Phys. Soc. Japan **19**, 1915 (1964).

[6] J. Rubinstein and J. G. Laframboise, Phys. Fluids **25**, 1174 (1982).

[7] A. Barjatya, C. M. Swenson, and D. Hysell, in *AGU Fall Meeting, San Francisco, California* (2005).

[8] K. I. Oyama, Planet. Space Sci. **24**, 183 (1976).

[9] A. Piel, M. Hirt, and C. T. Steigies, J. Phys. D: Appl. Phys. **34**, 2643 (2001).

[10] D. Strele, M. Koepke, R. Schrittweiser, and P. Winkler, Rev. Sci. Instrum. **68**, 3751 (1997).

[11] W. E. Amatucci, P. W. Schuck, D. N. Walker, P. M. Kintner, S. Powell, B. Holbeck, and D. Leonhardt, Rev. Sci. Instrum. **72**, 2052 (2001).

[12] I. Langmuir and H. M. Mott-Smith, Gen. Elec. Rev. p. 616 (1924).

[13] H. M. Mott-Smith and I. Langmuir, Phys. Rev. **28**, 727 (1926).

[14] F. F. Chen, in *Plasma Diagnostic Techniques*, edited by R. Huddlestone and S. Leonard (Academic Press, New York, 1965), pp. 113–200.

[15] J. D. Swift and M. J. R. Schwar, *Electrical Probes for Plasma Diagnostics* (Iliffe Books, London, 1970).

[16] N. Hershkowitz, in *Plasma Diagnostics*, edited by O. Auciello and D. Flamm (Academic Press, New York, 1989), vol. 1, pp. 113–184.

[17] L. Schott, in *Plasma Diagnostics*, edited by W. Lochte-Holtgreven (AIP Press, New York, 1995), pp. 668–731.

[18] W. R. Hoegy and L. E. Wharton, J. Appl. Phys **44**, 5365 (1973).

[19] I. Katz, G. Jongeward, V. Davis, T. Morton, and D. Ferguson, in *Measurement Techniques in Space Plasmas: Particles*, edited by R. F. P. et al. (AGU, Washington, D.C., 1998), vol. 102 of *Geophysical Monograph Series.*, pp. 37–41.

[20] L. W. Parker and B. L. Murphy, J. Geophys. Res. **72**, 1631 (1967).

[21] J. R. Sanmartin, Phys. Fluids **13**, 103 (1970).

[22] I. Katz, G. Jongeward, V. Davis, M. Mandell, R. Kuharski, J. Lilley, W. Raitt, D. Cooke, R. Torbert, G. Larson, et al., J. Geophys. Res. **94**, 1450 (1989).

[23] W. B. Thompson, in *Spacecraft Environmental Interactions Technology, AFGL-TR-85-0018/NASA Conf. Publ. 2359*, edited by C. Purvis and C. Pike (1983), pp. 649–662.

[24] J. G. Laframboise and L. J. Sonmor, J. Geophys. Res. **98**, 337 (1993).

[25] J. E. Jackson and J. A. Kane, J. Geophys. Res. **64**, 1074 (1959).

[26] K. G. Balmain, IEEE Trans. Antennas Propagat. **AP-17**, 389 (1969).

[27] R. H. Bishop, Ph.D. thesis, University of Utah, Salt Lake City (1970).

[28] J. Ward, C. M. Swenson, and C. Furse, IEEE Trans. Antennas Propagat. **53**, 2711 (2005).

[29] K. G. Balmain and G. A. Oksiutik, in *Plasma Waves in Space and in the Laboratory*, edited by J. Thomas and B. Landmark (American Elsevier, New York, 1969), vol. 1, pp. 247–261.

[30] K. D. Baker, J. Labelle, R. F. Pfaff, L. C. Howlett, N. B. Rao, J. C. Ulwick, and M. C. Kelley, J. Atmos. Terr. Phys. **47**, 781 (1985).

[31] C. T. Steigies, D. Block, M. Hirt, B. Hipp, A.Piel, and J. Grygorczuk, J. Phys. D: Appl. Phys. **33**, 405 (2000).

[32] A. Barjatya and C. M. Swenson, J. Geophys. Res. **111, A10302, doi:10.1029/2006JA011806** (2006).

[33] COSPAR and URSI, *International reference ionosphere home page*, [http://modelweb.gsfc.nasa.gov/ionos/iri.html] (2001).

[34] D. Bilitza, W. R. Hoegy, L. H. Brace, and R. F. Theis, Adv. Space Res. **8**, 209 (1988).

[35] L. Scherliess, R. W. Schunk, J. J. Sojka, D. C. Thompson, and L. Zhu, J. Geophys. Res. **111, A11315, doi:10.1029/2006JA011712** (2006).

[36] D. C. Ferguson, G. B. Hillard, T. L. Morton, and R. Peterson, in *41st Aerospace Sciences Meeting and Exhibit, Reno, Nevada* (2003), pp. AIAA–2003–1083.